Inner-Shell Water Rearrangement Following Photo-Excitation of Tris(2,2′-bipyridine)iron(II)

Journal:	*The Journal of Physical Chemistry*
Manuscript ID	jp-2015-10980j.R1
Manuscript Type:	Article
Date Submitted by the Author:	11-Dec-2015
Complete List of Authors:	Das, Akshaya; University of Basel, Chemistry Solomon, Rajadurai; University of South Carolina, Department of Chemical Engineering Hofmann, Franziska; University, Chemistry Meuwly, Markus; University, Chemistry

Inner-Shell Water Rearrangement Following Photo-Excitation of Tris(2,2′-bipyridine)iron(II)

Akshaya K. Das, R. V. Solomon, Franziska Hofmann,and Markus Meuwly**

Department of Chemistry, University of Basel, Klingelbergstrasse 80, Basel, Switzerland

E-mail: m.meuwly@unibas.ch

Phone: +41 (0)61 267 38 21. Fax: +41 (0)61 267 38 55

Abstract

The solvent dynamics in Fe-tris-bipyridine $[Fe(bpy)_3]^{2+}$ upon electronic excitation (oxidation) and subsequent relaxation is followed on the picosecond time scale by using atomistic simulations. Starting from the low spin (LS) $Fe(II)_{LS}$ state the transition to the excited Fe(III) ^{1,3}MLCT (metal-to-ligand charge transfer) state decreases the water coordination in immediate proximity of the central iron atom. This readjustment of the solvent shell occurs on the sub-picosecond time scale. Full relaxation of the water environment would occur on the 10 ps time scale which is, however, never reached as the lifetime of the ^{1,3}MLCT state is only 200 fs. Further relaxation towards the long-lived (665 ps) $[Fe(II)_{HS}(bpy)_3]$ high spin (HS) state does not change the degree of solvation. The results support a model in which the change in the degree of solvation is driven by electronic effects (charge redistribution) and not by structural changes (change in bond lengths). Furthermore, the results are consistent with recent combined X-ray emission (XES) and X-ray diffusion (XDS) scattering experiments which provided evidence for a reduced solvent density upon excitation of the $[Fe(II)_{LS}(bpy)_3]$ initial state. However, the time scale for water exchange dynamics is faster than that found in the experiments.

*To whom correspondence should be addressed

1 Introduction

Iron-containing complexes constitute an important and versatile class of metal complexes. Depending on the strength of the ligands they can exist either in a low (LS) or in a high spin (HS) state. Specifically, the [Fe(II)(bpy)$_3$] complex exhibits two spin states: a LS singlet (^{1}A$_1$) and a HS quintet (^{5}T$_2$).[1,2] Between these two states, excited state charge transfer and spin dynamics takes place (spin crossover - SCO - dynamics) which can be induced by illumination, temperature or pressure changes.[3] Switchable transition metal-based systems are potentially interesting for applications in solar cells, data storage or in molecular devices. Often, they are based on ruthenium which is, however, rare and toxic. Iron would be an attractive replacement but due to the very short-lived excited states it has as yet not been widely used for solar energy conversion. However, there has been recent progress with an iron-nitrogen-heterocyclic-carbene compound.[4]

In solution, the SCO process involves a first inter system crossing (ISC) to a metal-to-ligand-charge transfer (^{1,3}MLCT) state followed by relaxation which brings the molecule to the HS state (see Figure 1), possibly via one or several triplet intermediates.[1] During the photo excitation energy is dissipated to the environment, potentially including intra-molecular degrees of freedom. However, following the non-equilibrium response of the surrounding solvent molecules towards equilibrium from experiment alone at atomistic scales is difficult. More generally, relating temporal information such as relaxation times to actual structural rearrangements can be very challenging. One example for which this has been attempted is the dynamics of photodissociated carbon monoxide in myoglobin for which the combination of time resolved Laue diffraction and infrared spectroscopy provided information which relates structural changes with spectroscopic response.[5,6] In structural dynamics, time scales from 2-dimensional infrared spectroscopy of solvated cyanide could be related to water exchange dynamics in the solvent shell from analysis of atomistic simulations using accurate force fields.[7]

For $Fe(bpy)_3$, earlier work based on the analysis of time resolved X-ray spectroscopy experiments suggests that during SCO one to two water molecules are pushed out of the first solvent shell between the $[Fe(II)_{LS}(bpy)_3]$ and $[Fe(II)_{HS}(bpy)_3]$ states on the 100 ps time scale.[3] Also, an *ab initio* mixed quantum mechanics/molecular mechanics (QM/MM) simulation involving the same two states reveals that the solvent shell around the two states differs by two water molecules.[8] However, both studies did not relate actual structural changes with the time scales involved at atomic resolution.

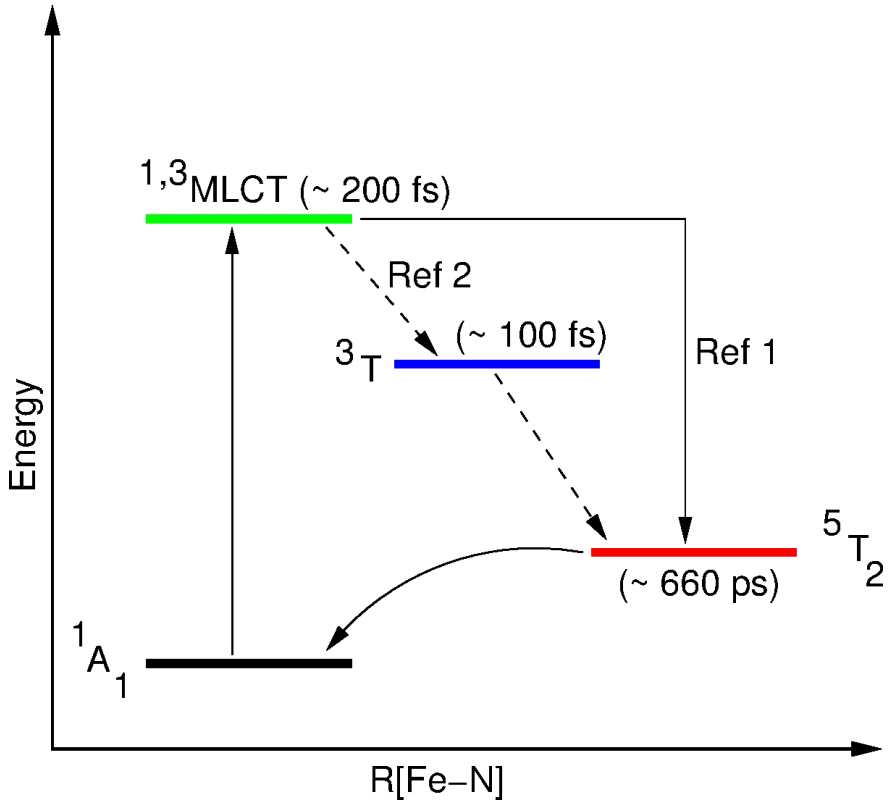

Figure 1: Schematic for SCO involving the aqueous $[Fe(II)(bpy)_3]$ complex. The process studied here occurs along the solid arrow. The dashed lines are additional processes on the sub-picosecond time scale analyzed in previous work.[2] The lifetime of each state is reported in brackets. Intermediate triplet states ($^3T_1$) and ($^3T_2$) are labelled as ^3T.

Solvent molecules around metal complexes are of fundamental and practical relevance both, in catalysis and in solar energy conversion.[9–12] However, directly observing and characteriz-

ing the influence and role of solvent is difficult experimentally mainly because of the transient nature of the process and the finite time resolution of the experiments. Computational approaches applied to metal-containing systems have become more widespread recently due to both, increased computing power and technological advances. Amongst others, tight-binding schemes have been extended to treat copper complexes.[13] Furthermore, force field-based techniques have been successfully applied to the investigation of a range of metal-containing systems.[14–19]

For $Fe(bpy)_3$ the experimental information provided so far is indirect[3] and only one QM/MM trajectory, approximately 25 and 4 ps in length for the LS and HS states, respectively, could be run due to the considerable computational effort of such simulations.[8] Typical experiments provide ensemble-averaged observables, which require statistical averaging over many independent trajectories in the simulations for direct comparison, which is usually not possible with QM/MM simulations of metal-containing systems. In the present work computational strategies are employed which allow rigorous sampling by using valence-bond-based force fields for the species involved. This allows to follow the atomistic dynamics for hundreds of trajectories over extended time scales. First, the force field is validated vis-a-vis experimental structures and infrared frequencies. In a next step, the solvation dynamics of the ground- and excited-state species is followed from equilibrium and non-equilibrium MD simulations.

2 Methods

2.1 Computational Details

All MD simulations were carried out with the CHARMM[20] program, the CHARMM22[21] force field and provisions for VALBOND.[17] The VALBOND force field is based on valence bond theory and capable to more realistically describe angle bending in metal complexes.[22–24]

For this, the harmonic bending energy term in a conventional force field for an L1-M-L2 motif is replaced by a parameterization which depends on the overlap of the hybrid orbitals on the central metal atom, where L1 and L2 are ligands and M is the metal atom. Unlike the simple harmonic approximation, VALBOND bending functions capture the energetics at very large angular distortions and support hypervalent compounds by means of 3-center-4-electron bonds.[23] The remaining parameters for the bipyrimidine rings were those from the CHARMM22[21] and CHARMM General Force Field (CGenFF[25]).

For the present study, three complexes [Fe(II)$_{\mathrm{LS}}$(bpy)$_3$], [Fe(II)$_{\mathrm{HS}}$(bpy)$_3$] and [Fe(III)(bpy)$_3$] were considered. Their structures were optimized and natural bond orbital (NBO)[26] charges were determined using Gaussian09[27] with the 6-31G(d,p)[28] basis set at the B3LYP[29] level of theory. Partial charges on each atom of the ligand and metal atom, for all three systems are summarized in Table 1. The van der Waals parameters for Fe are those from 6-coordinate heme[30] ($R_{\mathrm{min}}/2$ = 0.65 Å and $\epsilon = -0.01$ kcal/mol) although additional simulations were carried out with $\epsilon = -0.5$ kcal/mol but no differences were found. This is not too surprising as the Fe-atom is deeply buried within the complex and only electrostatic interactions are expected to be of importance for the interaction with the solvent.

Table 1: NBO charges (in units of e) for the three states of the metal complex obtained from the *ab initio* calculations. For labelling of the atom types see Figure 3.

Atoms	Fe(II)$_{\mathrm{LS}}$	Fe(II)$_{\mathrm{HS}}$	Fe(III)
FEX	0.98	1.33	1.21
NX	–0.49	–0.55	–0.50
CE2	0.18	0.19	0.19
CA1	0.04	0.05	0.06
CA2	–0.25	–0.26	–0.23
CA3	–0.17	–0.17	–0.13
CA4	–0.22	–0.23	–0.21
HP	0.27	0.27	0.28

As a first validation, the global structures of the optimized structures from electronic struc-

ture and force field calculations were compared with experiment. For this, all mutual atom-atom distances were computed for the $Fe(II)_{LS}$ and Fe(III) complexes and compared with the experimental crystal data (see Figure 2).[31–34] It is found that the VALBOND optimized geometries favorably agree with experimental crystal structures.[34] Since the crystal structure of $[Fe(II)_{HS}(bpy)_3]$ is not available, its VALBOND force field optimized geometry is compared with the optimized structure from the *ab initio* calculations. Table 2 provides a comparison of the most relevant average bond lengths for the three complexes obtained from force field and *ab initio* calculations with the reference structures. It is confirmed that the present force fields faithfully reproduce the structures of the $[Fe(II)_{LS}(bpy)_3]$, $[Fe(II)_{HS}(bpy)_3]$ and $[Fe(III)(bpy)_3]$ complexes.

Table 2: Bond length comparison for $[Fe(II)_{LS}(bpy)_3]$, $[Fe(III)(bpy)_3]$ and $[Fe(II)_{HS}(bpy)_3]$ obtained from FF, *ab initio* (B3LYP/6-31G(d,p)) and experiment.[31–34]

	$Fe(II)_{LS}$			Fe(III)			$Fe(II)_{HS}$	
Bond Type	CHARMM (Å)	*ab initio* (Å)	Expt. X-ray (Å)	CHARMM (Å)	*ab initio* (Å)	Expt. X-ray (Å)	CHARMM (Å)	*ab initio* (Å)
CA - CA	1.375	1.391	1.37-1.39	1.375	1.393	1.37	1.410	1.390
CA - HP	1.080	1.083		1.080	1.083	0.94	1.080	1.083
CA - CE2	1.397	1.397		1.395	1.395	1.38	1.427	1.400
CE2 - CE2	1.476	1.476	1.47	1.471	1.471	1.47	1.493	1.485
CA - NX	1.347	1.343	1.34-1.36	1.346	1.346	1.35	1.357	1.345
CE2 - NX	1.364	1.357	1.34-1.36	1.360	1.361	1.36	1.376	1.357
FEX - NX	2.022	2.022	1.95,1.97	2.005	2.005	1.96	2.200	2.188

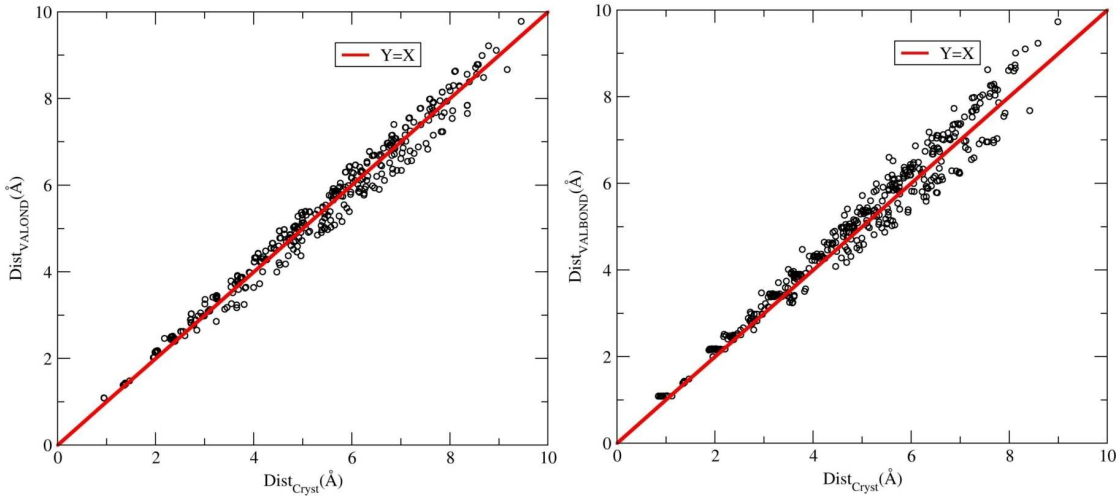

Figure 2: Comparison of atom-to-atom distance between the VALBOND force filed optimized geometry and experimental crystal structure for $[Fe(II)_{LS}(bpy)_3]$ (left) and $[Fe(III)(bpy)_3]$ (right).

Furthermore, to validate the non-bonded parameters, interaction energies between one water molecule and the metal complex were computed for 50 different configurations extracted from a low-temperature (50 K) MD simulation of 50 ps length. Interaction energies were compared with those obtained from *ab initio* calculations at the B3LYP/6-31G(d,p) level of theory and the correlation coefficient was $R^2 = 0.98$ with a slope of 0.97 for the linear fit. This provides further validation for the force field used.

The computational setup for the present study consists of the solvated iron complexes in a pre-equilibrated cubic box of size 37.25 Å containing 1694 water molecules, with 5143 atoms in total (see Figure 3). Periodic boundary conditions (PBC) were applied. The non-bonded interactions (electrostatic and Lennard-Jones) were truncated at a distance of 14 Å and switched between 10 and 12 Å. First, the species of interest - solvated $[Fe(II)_{LS}(bpy)_3]$, $[Fe(II)_{HS}(bpy)_3]$ and $[Fe(III)(bpy)_3]$ - were heated and equilibrated for 20 ns at 300 K. Newton's equations of motion were propagated in the NVT ensemble with a Verlet integrator. The water model used in the present work is the standard TIP3P model[35] and all bonds involving hydrogen atoms were constrained by applying SHAKE.[36] The time step used in

the simulations was $\Delta t = 1$ fs.

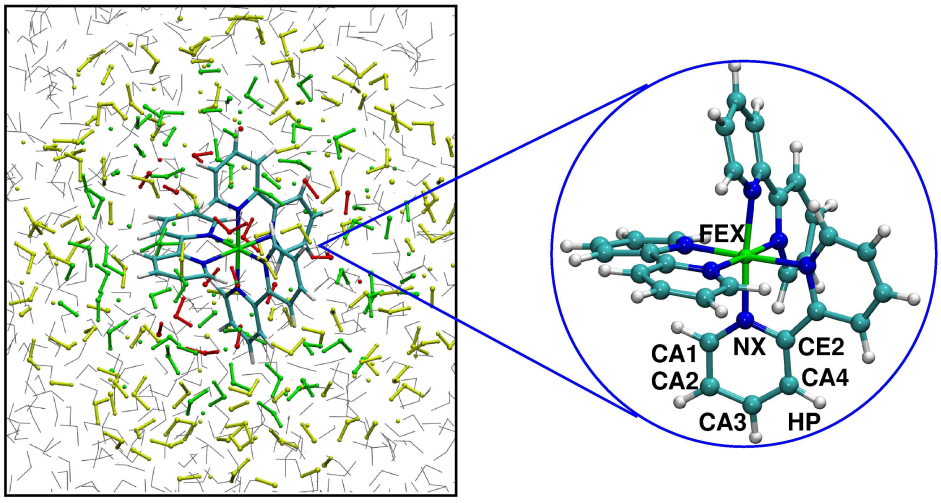

Figure 3: The simulation system, consisting of the $[Fe(II)_{LS}(bpy)_3]$ complex and the solvation environment. Water molecules in the first solvation layer at 6.3 Å are shown in red color, second shell at 9.0 Å in green color, third shell at 11.6 Å in yellow color and bulk water in gray lines. Atom color code: Carbon (cyan), Nitrogen (blue), Iron (green) and Hydrogen (white).

After preparation, equilibrium simulations for the $Fe(II)_{LS}$, $Fe(II)_{HS}$ and Fe(III) compounds were carried out in order to determine reference equilibrium properties including the energetics, the radial distribution function (RDF) $g(r)$, and $N(r)$ which is the number of water molecules as a function of the distance r of water-oxygen atoms from the Fe-atom. The structures and velocities along the $Fe(II)_{LS}$ and Fe(III) equilibrium trajectory also served as initial conditions for the non-equilibrium simulations. Overall, 100 initial structures were generated, each separated by 10 ps from each other. Electronic excitation from $Fe(II)_{LS}$ to Fe(III) was induced by instantaneously changing the force field parameters between the two oxidation states (denoted as $Fe(III)^{neq}$). Similarly, the relaxation process of Fe(III) to $Fe(II)_{HS}$ was carried out by changing the force field parameters from Fe(III) to $Fe(II)_{HS}$ (labeled $Fe(II)^{neq}_{HS}$). Such perturbations lead to a non-equilibrium situation from which the system relaxes towards an equilibrium state. Each non-equilibrium simulation was run for 25 ps.

2.2 Trajectory Analysis

From the temporal evolution of the coordinates and velocities following observables are calculated.

Radial distribution functions: Radial distribution functions $g(r)$ were computed from the distance-time series of the respective coordinate r for each trajectory obtained from the MD simulation and then averaged over all. $g_{\mathrm{O}}(r)$ and $g_{\mathrm{H}}(r)$ were computed by considering Fe-O_W and Fe-H_W respectively. O_W and H_W corresponds to the water oxygen and water hydrogen. From the $g(r)$, corresponding $N(r_s)$ for a given solvent shell (up to distance r_s) was computed using equation 1

$$N(r_s) = 4\pi\rho \int_0^{r_s} r^2 g(r) dr \tag{1}$$

where ρ is the bulk water density. $N_{\mathrm{H}}(r)/N_{\mathrm{O}}(r)$ was also computed to account the organization of water molecules around the metal center. In particular, it provides orientational preference of water molecules around the complex. $N_{\mathrm{H}}(r)/N_{\mathrm{O}}(r) = 2$ corresponds to the bulk water. If the value different from 2 suggests structuring of water molecules around metal complex.

Rotational reorientation times of water: The rotational reorientation time τ_r of a water molecule is computed by fitting an exponential function $R_r(t) = A\exp(-t/\tau_r)$ to the rotational time correlation function computed using $R_r(t) =< \vec{u}(0)\vec{u}(t) >$. All the rotational reorientation time calculations were carried out within the CHARMM program.[20]

Water residence times: Exchange dynamics of water molecules around the metal complex

was analyzed by computing their residence time in the different shells as characterized by the radial distribution functions. For a given solvent shell, the residence time is determined from the time correlation function $R(\tau)$[37,38]

$$R(\tau) = \frac{1}{N n_W} \sum_{i=1}^{N} \sum_{j=1}^{n_W} \Theta_j(t)\Theta_j(t+\tau) \tag{2}$$

which was fitted to a bi-exponential function (see equation 3). In Equation 2 N is the number of trajectories, $\Theta_j(t)$ is the step function which describes the presence of a water molecules j in a given shell and n_W is the number of water molecules in the respective shell. If the water molecule j is present in the shell, then $\Theta_j(t) = 1$, otherwise $\Theta_j(t) = 0$. The spatial extent of the water shells r_s are defined by the minima of $g_{\mathrm{O}}(r)$ and a water molecule is considered to belong to a particular shell for $r \leq r_s$.

$$R_2(\tau) = A_1 \exp\left(-\frac{t}{T_1}\right) + A_2 \exp\left(-\frac{t}{T_2}\right) \tag{3}$$

The two time constants T_1 and T_2 provide information about the dynamics of water molecules close to the border of the shell and the typical lifetime within a shell and A_1 and A_2 describe the relative importance of each processes.

IR spectra: Vibrational spectra $C(\omega)$ are obtained from the Fourier transform of the dipole-dipole auto-correlation function $C(t)$[39] which was averaged over 2^{15} time steps. The Fourier transform was computed using a Blackman filter.[40] Finally, the IR spectrum is computed using equation 4

$$A(\omega) \propto \omega(1 - \exp(-\hbar\omega/(k_B T)))C(\omega) \tag{4}$$

where $\hbar$ and k_B are the Planck and Boltzmann constant, respectively, and T is the simulation temperature.

3 Results and Discussion

3.1 Validation of the Force Field

Before investigating the equilibrium and non-equilibrium dynamics in more detail, the current force fields are further validated by comparing with experimental data. The structural comparison and validation of interaction energies between the complex and a water molecule has already been described above. Furthermore, the infrared spectrum of the $[Fe(II)_{LS}(bpy)_3]$ complex has been investigated experimentally and provides additional reference data for comparison. Table 3 summarizes the experimentally measured and computed line positions. There is a shift of ≈ 10 cm^{-1} for the Fe-N and ≈ 100 cm^{-1} for the C-N stretching frequency compared to the experiment, whereas for the C-C stretch this shift is ≈ 50 cm^{-1}.[32,41] These differences could be reduced by slightly modifying the force constants which was, however, not deemed necessary for the current work which is primarily concerned with the solvation dynamics *around* the complex. In the experiments, peaks for the stretching modes are reported to be at 423 cm^{-1} for Fe-N, 1605 cm^{-1} for C-C, 1470 cm^{-1} for C-N and 3080 cm^{-1} for C-H. To further validate the parametrization, the IR spectrum of the ^{15}N isomer is determined and overlapped with the spectrum for the normal isomer. It is found that there is ≈ 5 cm^{-1} of isotopic shift for the Fe-N stretch is in good agreement with a previously reported value of 6 cm^{-1}.[42] For the $[Fe(II)_{HS}(bpy)_3]$ complex no experimental data is available but electronic structure calculations on both Fe(II) complexes suggest only small changes in the vibrational frequencies[32] which is also found from the present simulations.

Table 3: Experimental[32,41] and computed IR spectrum of $[Fe(II)_{LS}(bpy)_3]$.

Assignment	Computed frequency cm^{-1}	Experimental frequency cm^{-1}
Fe-N	415	423
C-N	1370	1470
C-C	1555	1605

3.2 Equilibrium simulations

In a next step, the equilibrium dynamics of the solvated complexes is considered. The water structuring can be characterized by the Fe-O_W and Fe-H_W RDFs $g_O(r)$ and $g_H(r)$. Their integration provides the running coordination numbers $N_O(r)$ and $N_H(r)$, as described in the Methods section.

The radial distribution function $g_O(r)$ and corresponding coordination number $N_O(r)$ of water oxygen with respect to the Fe atom for all three equilibrium simulations $Fe(II)^{eq}_{LS}$, $Fe(II)^{eq}_{HS}$ and $Fe(III)^{eq}$ are shown in Figure 4. For $Fe(II)^{eq}_{LS}$ the first peak in $g_O(r)$ appears at 4.5 Å and a minimum at 5 Å describes the inner solvent shell close to the complex and the peak in the $g_O(r)$ is due to the interaction of the water hydrogen (H_w) with the negatively charged bipyridyl ring and water oxygen with the metal atom. This peak is less pronounced for $Fe(II)^{eq}_{HS}$ and disappears completely for $Fe(III)^{eq}$ (see Figure 4) because the amount of negative charge on each ring of the bipyridyl ligand decreases from -0.90 to $-0.83e$ in going from $Fe(II)^{eq}_{LS}$ to $Fe(III)^{eq}$ (see Table 1). This also lowers the interaction energy between H_w and the ring. Although the negative charge on the ring for $Fe(II)^{eq}_{HS}$ ($-0.94e$) is larger compared to $Fe(II)^{eq}_{LS}$, the peak is less pronounced due to the increased Fe-N bond length by 0.2 Å. A second maximum in $g_O(r)$ appears at 5.7 Å and a minimum at 6.3 Å, defines the first solvent shell (shell-I) around the Fe atom and this peak appears in all three cases. The running coordination number $N_O(r)$ in the same figure shows that there are 3 and 15 water molecules present in the inner and first solvent shell for $Fe(II)^{eq}_{LS}$. This is in good agreement with previous simulations on $[Ru(II)(bpy)_3]$ and $[Fe(II)(bpy)_3]$.[8,19] However, for $Fe(III)^{eq}$ there are 2 and 15 water molecules present in the inner and first solvent shell, respectively (see Figure 4).

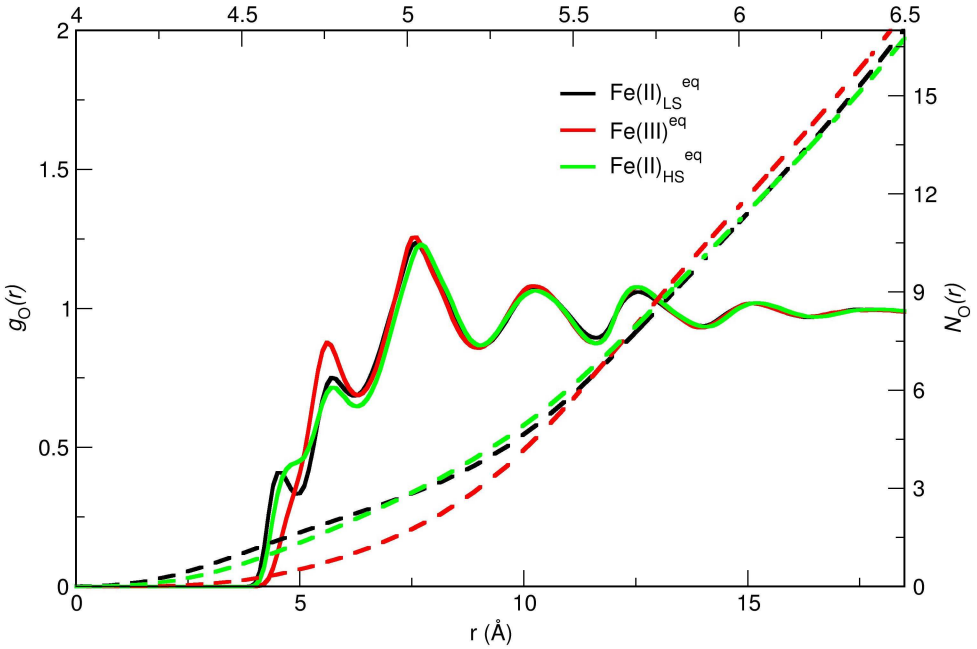

Figure 4: Radial distribution function $g_{\mathrm{O}}(r)$ (solid black, red and green lines, lower $x-$axis with left $y-$axis) and running coordination number $N_{\mathrm{O}}(r)$ (dashed black, red and green lines, upper $x-$axis with right $y-$axis) of water oxygen with respect to the Fe atom obtained from the all three equilibrium simulations $\mathrm{Fe(II)}^{\mathrm{eq}}_{\mathrm{LS}}$, $\mathrm{Fe(II)}^{\mathrm{eq}}_{\mathrm{HS}}$ and $\mathrm{Fe(III)}^{\mathrm{eq}}$ are shown.

The total charge on each bipyridyl ring is $-0.90e$, $-0.95e$, $-0.83e$ for $\mathrm{Fe(II)}_{\mathrm{LS}}$, $\mathrm{Fe(II)}_{\mathrm{HS}}$ and Fe(III), respectively, which yields an electrostatic component of the interaction energy between the closest water molecule and the complex of –6.87, –6.52 and –2.93 kcal/mol for LS, HS and Fe(III) in their energy minimized structures. For all three systems the water-hydrogen H_w always points towards the bipyridyl ring. For a direct comparison, the energetics of the optimized structure of the $\mathrm{Fe(II)}_{\mathrm{LS}}$ was also analyzed. The interaction energy between a single water molecule and the complex for the three states is –6.87, –6.35 and –2.78 kcal/mol for LS, HS and Fe(III) respectively. The electrostatic interaction between the water molecule and the metal atom are 8.02, 10.92 and 9.99 kcal/mol for LS, HS and Fe(III), respectively, whereas for the ligands in the absence of the metal atom they are –14.88, –17.27 and –12.77 kcal/mol.

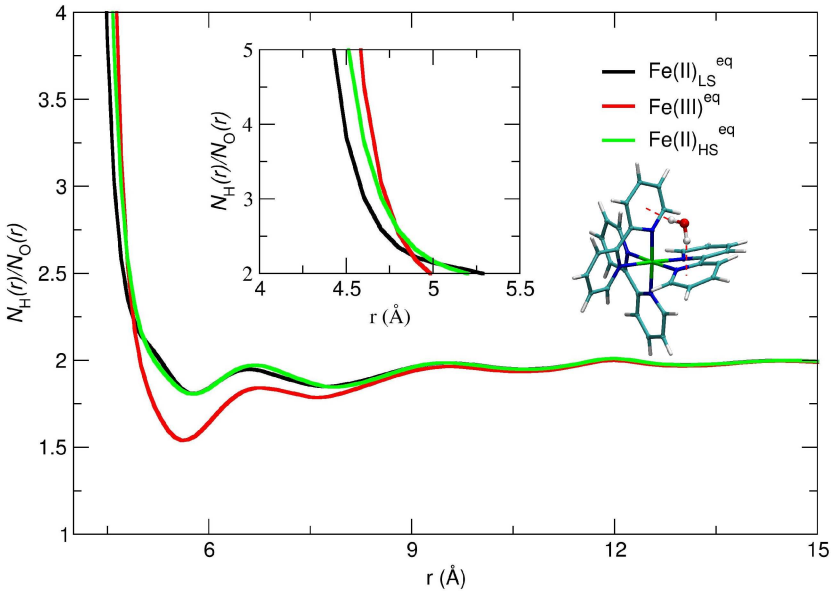

Figure 5: Ratio of running coordination number of water oxygen and water hydrogen with respect to Fe atom obtained from three equilibrium simulations. Inset shows the $N_{\mathrm{H}}(r)/N_{\mathrm{O}}(r)$ ratio in the inner shell and the complex with water molecule shows the preferred orientation of water inside the groove of the complex in $\mathrm{Fe(II)}_{\mathrm{LS}}^{\mathrm{eq}}$.

Additional information regarding the organization of the water molecules can be obtained from analyzing the ratio $N_{\mathrm{H}}(r)/N_{\mathrm{O}}(r)$ (see Figure 5). In bulk water, this ratio is $N_{\mathrm{H}}(r)/N_{\mathrm{O}}(r) = 2$. However, due to orientational preference around a solute molecule, it can deviate considerably from this idealized value. At short distances from the metal center there is an over-proportion of hydrogen atoms which can be rationalized from the structure reported in Figure 5. With increasing distance there are slightly more oxygen atoms until the bulk value of $N_{\mathrm{H}}(r)/N_{\mathrm{O}}(r) = 2$ is reached for separations larger than about 12 Å.

Within 5 Å from the metal atom $N_{\mathrm{H}}(r)/N_{\mathrm{O}}(r) > 2$ for all three systems (see Figure 5) due to the orientation of $\mathrm{H_w}$ towards the center of the complex, the interaction of $\mathrm{H_w}$ with the negatively charged bipyridyl ring and the smaller van der Waals radius $R_{min}/2 = 0.2245$ Å). Around the second maximum of $g_{\mathrm{O}}(r)$ at 6.3 Å, $N_{\mathrm{H}}(r)/N_{\mathrm{O}}(r) < 2$ (1.79 for $\mathrm{Fe(II)}_{\mathrm{LS}}^{\mathrm{eq}}$, 1.81 for $\mathrm{Fe(II)}_{\mathrm{HS}}^{\mathrm{eq}}$ and 1.5 for $\mathrm{Fe(III)}^{\mathrm{eq}}$), reflecting the fact that an over-proportion of water-oxygens are oriented towards the center of the iron complex (i.e. depletion of H-atoms), and

then approaches the bulk-value of $N_{\mathrm{H}}(r)/N_{\mathrm{O}}(r) = 2$ asymptotically. The difference between $N_{\mathrm{H}}(r)/N_{\mathrm{O}}(r)$ for $\mathrm{Fe(II)}^{\mathrm{eq}}_{\mathrm{LS}}$ and $\mathrm{Fe(III)}^{\mathrm{eq}}$ remains always above 0.2 for distances up to $r \approx 6$ Å which suggests that the proportion of hydrogen atoms for $\mathrm{Fe(II)}^{\mathrm{eq}}$ is larger compared to $\mathrm{Fe(III)}^{\mathrm{eq}}$. This reflects the stronger electrostatic interaction between the water molecule and the ligand for Fe(II) compared to Fe(III). In going from $\mathrm{Fe(II)}^{\mathrm{eq}}_{\mathrm{LS}}$ to $\mathrm{Fe(II)}^{\mathrm{eq}}_{\mathrm{HS}}$, the value of $N_{\mathrm{H}}(r)/N_{\mathrm{O}}(r)$ (1.79 for $\mathrm{Fe(II)}^{\mathrm{eq}}_{\mathrm{LS}}$ and 1.81 for $\mathrm{Fe(II)}^{\mathrm{eq}}_{\mathrm{HS}}$) remains almost unchanged (see Figure 5) due to the very similar interaction energies with the solvent. For a distance of $r = 9$ Å from the metal atom, the difference drops to approximately 0.05 and for $r = 12.5$ Å $N_{\mathrm{H}}(r)/N_{\mathrm{O}}(r) \approx 2$ which corresponds to bulk water.

Water reorientation times: The dynamics of the water molecules can be characterized by considering their rotational reorientation. Rotational reorientation times τ_r decrease gradually in going from the first solvent shell to bulk water, as the rotational dynamics of the solvent molecules close to the complex slows down. For bulk water, τ_r is 0.785 ps which is in good agreement with the previously reported value of 0.7 ps from simulations (TIP3P water model).[43] However it is slower compared to the experimental value of 1.95 ps.[44] For solvent molecules close to the metal complex τ_r increases by 30 % due to the interactions with the metal complexes.

Water residence times: The water residence times were computed using the procedure described in the method section and are given in Table 4. Two time constants T_1 and T_2 describe the dynamics, see Figure 6. T_1 in all three equilibrium simulations are similar (≈ 0.2 ps). This time scale characterizes the rapid recrossing dynamics at the border of the shell while T_2 is on the several ps time scale and represents the typical lifetime in a given water shell (shells I to III). For simulations of pure water with the MCY model this time has been reported to be 4.5 ps.[37] In previous work the short recrossings were eliminated by introducing a lag time t^* which was set to 2 ps.[37] For the first solvent shell, $T_2 = 3.78$ ps for

$Fe(II)^{eq}_{LS}$ which is larger compared to the other two equilibrium simulations and can be qualitatively explained by the increased electrostatic interaction between the water molecules and the complex (see above). Since T_2 describes the lifetime within a given shell and the shells grow in size, T_2 gradually increases with the shell radius due to an increase in the number of solvent molecules. In all three equilibrium simulations the residence time for shell-III is $\approx$ 11 ps (see Table 4) which is consistent with 12.2 ps and 12.4 ps found previously based on force field or mixed QM/MM simulation on aqueous $[Ru(II)(bpy)_3]$.[19,45]

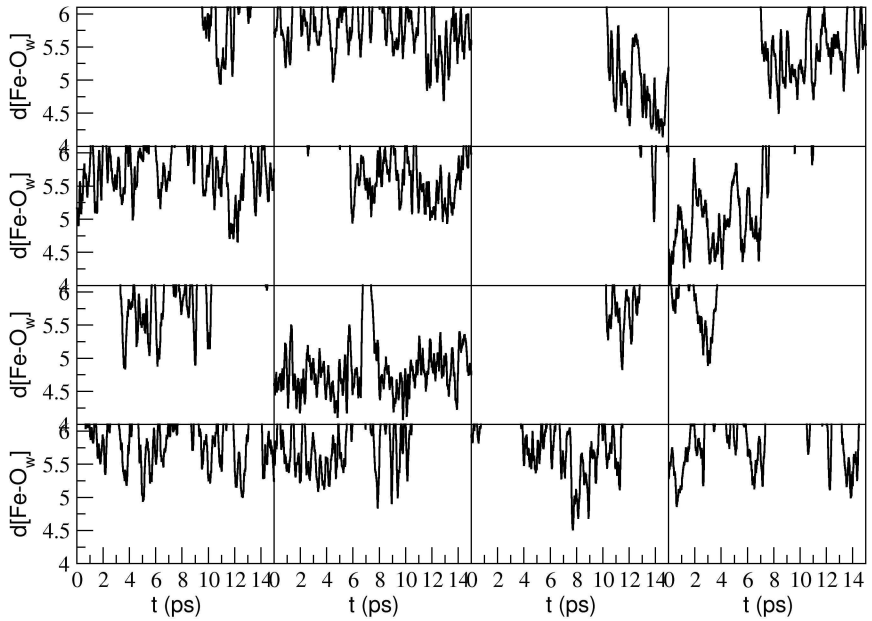

Figure 6: Distances of 16 water oxygen (involved in the exchange process) within 5 Å of the Fe atom during equilibrium simulations of $Fe(II)^{eq}_{LS}$.

The correlation function $C_O(t) =< \delta O(0)\delta O(t) > / < [\delta O(0)]^2 >$ determines the persistence time of a particular water shell (see Figure 7). Here $O(t) = 1$ for all water oxygen atoms if they are within a distance R of the Fe-atom, otherwise $O(t) = 0$. $C_O(t)$ was computed by considering all water oxygen atoms for which $O(t) = 1$ at least once during the whole simulation. In other words, $C_O(t)$ describes the persistence time of a particular solvent shell. For shell-I (at 6.3 Å) and one particular simulation of $Fe(II)^{eq}_{LS}$, a bi-exponential function

fitted to $C_{\mathrm{O}}(t)$ yields two time constants 5.3 and 39.8 ps (see Figure 7). The first time constant characterizes exchange of one water molecule between neighboring shells for this specific simulation and the second time constant is the time required for the complete exchange of water molecules in this shell. Following the complete dynamics of all shell-I water molecules starting from an arbitrary snapshot yields a time of 20 ps for full replacement by water molecules from solvent molecules further away. Also, the magnitude of the longer time scale is consistent with previous work on CN^- for which complete replacement of the first water shell (10 water molecules) was found to occur on the 10 ps time scale.[7] Hence, for $Fe(II)^{eq}_{LS}$, the diffusion and replacement of solvent molecules between neighboring shells occurs on the picoseconds time scale (see Figure 7).

Explicit analysis of 15 ps of simulations for $Fe(II)^{eq}_{LS}$ yields ≈ 20 water molecules that are involved in the exchange process within 5 Å from the Fe atom and their distances from the metal center are reported in Figure 6. Water molecules with short life times (< 1 ps) are those close to the boundary. The probability distribution of the life time of water molecules (> 1 ps) within 5 Å from the metal center were computed for $Fe(II)^{eq}_{LS}$ (see Figure 8) and yield $< \tau >= \frac{\sum_i p_i \tau_i}{\sum_i p_i} = 2.23$ ps which qualitatively agrees with the residence times (3.78 ps, see Table 4).

Table 4: Time constants for residence correlation functions $R(\tau)$ for the equilibrium simulations

	r_s (Å)	Shell-I $0< r_s \leq 6.3$	Shell-II $0< r_s \leq 9.0$	Shell-III $0< r_s \leq 11.6$
$Fe(II)^{eq}_{LS}$	No. of water	15	83	199
	A_1	0.668	0.679	0.666
	A_2	0.132	0.161	0.134
	T_1/ps	0.30	0.37	0.47
	T_2/ps	3.78	7.28	11.59
$Fe(II)^{eq}_{HS}$	No. of water	14	83	198
	A_1	0.652	0.679	0.664
	A_2	0.189	0.160	0.135
	T_1/ps	0.24	0.36	0.47
	T_2/ps	2.94	7.28	11.48
$Fe(III)^{eq}$	No. of water	15	83	199
	A_1	0.661	0.674	0.667
	A_2	0.198	0.161	0.133
	T_1/ps	0.22	0.36	0.47
	T_2/ps	2.45	7.08	11.59

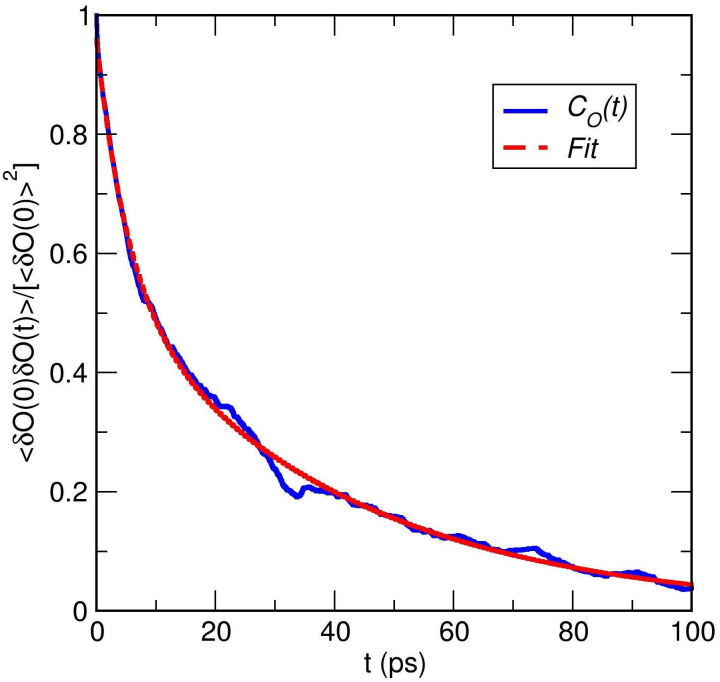

Figure 7: The occupation correlation function $C_{\mathrm{O}}(t)$ of $\delta O(t)$ as a function of time within the distance of 6.3 Å from the metal center for $Fe(II)^{eq}_{LS}$. The red dotted line is a bi-exponential fit.

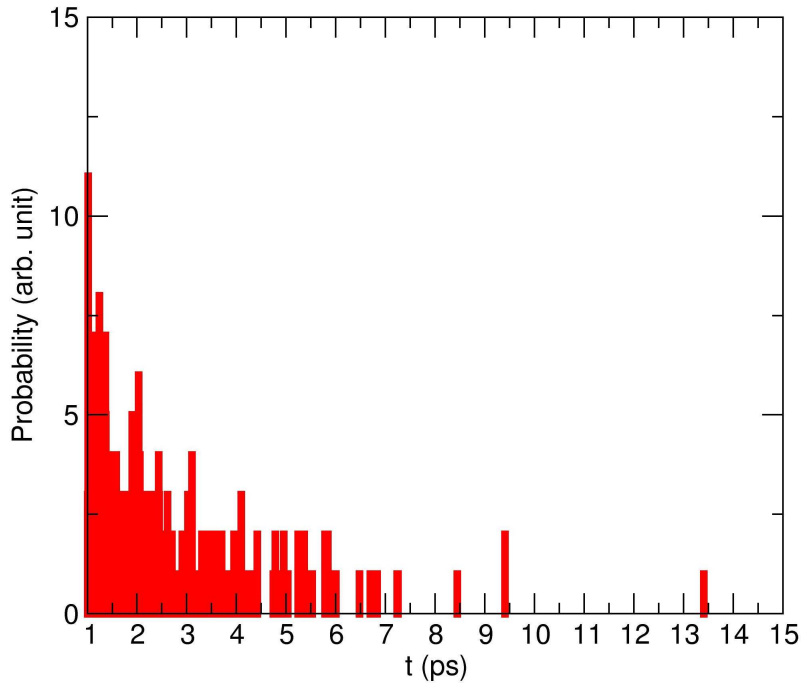

Figure 8: Survival probability distribution $p(\tau)$ for water molecules within 5 Å from the metal center in the equilibrium simulations of $\mathrm{Fe(II)}^{\mathrm{eq}}_{\mathrm{LS}}$.

3.3 Non-equilibrium simulations

For the investigation of the solvent reorganization dynamics depending on the oxidation state of the complex, photo-excitation was modeled by instantaneously changing the force field parameters from one state to the other (see Methods). Such a procedure has also been employed for CO- and NO-photodissociation from heme in Myoglobin[46] and for electronic excitation in ClCN.[47]

Structural Reorganization of the Solvent after Photoexcitation: To describe solvent structure rearrangement after photoexcitation of $\mathrm{Fe(II)(bpy)_3}$, the radial distribution function $g_{\mathrm{O}}(r)$ and the water-coordination number $N_{\mathrm{O}}(r)$ around the Fe-atom was analyzed. As mentioned previously and reported in Figure 4 the most pronounced difference in $g_{\mathrm{O}}(r)$ for all three states $\mathrm{Fe(II)}^{\mathrm{eq}}_{\mathrm{LS}}$, $\mathrm{Fe(II)}^{\mathrm{eq}}_{\mathrm{HS}}$ and $\mathrm{Fe(III)}^{\mathrm{eq}}$ is within 5 Å, see Figure 4. Since the differences in $g_{\mathrm{O}}(r)$ beyond 5 Å are rather small we focus only on the inner shell. The photocycle was

studied in three steps, first $Fe(II)_{LS}$ was excited to ^{1,3}MLCT and then it relaxed to $Fe(II)_{HS}$, subsequently it returns to the $Fe(II)_{LS}$ state, see Figure 1.[1] In the photo excitation of $Fe(II)_{LS}$ to ^{1,3}MLCT the degree of solvation decreases by less than one water molecules depending on the distance from the iron atom considered. There is no substantial change in the degree of solvation in the other two relaxation processes (see Figures 9 and 11).

For more insight into the time scale for the geometrical relaxation of solvent structure around the metal center, the coordination number at different times after photo-excitation, relaxation and SCO were determined. Since $N_O(r)$ between the systems differs most at 4.75 Å, this value was used in the analysis. To quantify the time scale for solvent reorganization, a single exponential function was fit to this data in and yields a decay constant of 0.80 and 2.81 ps for $Fe(III)^{neq}$ and $Fe(II)^{neq}_{HS}$, respectively, see Figure 10. Such relaxation times agree well with recent experiments which found 1.1 and 3.4 ps from transient absorption spectroscopy.[48] Hence, in all three cases, the geometrical relaxation of the solvent occurs on the ps time scale (see Figure 10). This has also been investigated for systems such as I^-/I^0 in water for which QM/MM simulations and XAS experiments[49,50] have been carried out. The computations yield reorganization times of 3 to 4 ps whereas the picosecond experiments with a time resolution of 70 ps are too slow to be sensitive to the solvent reorganization. Overall, the time scale of the process obtained from the computationally much more demanding QM/MM simulations on solvated halides compare favorably with those reported in the present work.

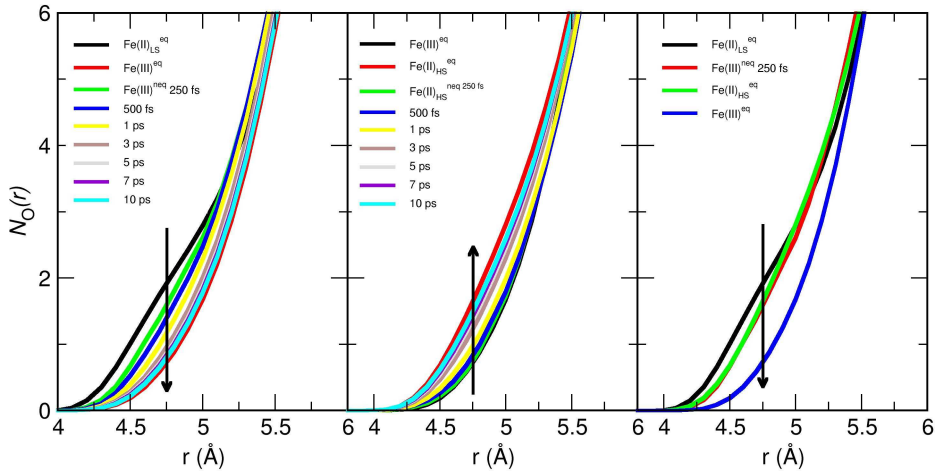

Figure 9: Running coordination number $N_{\mathrm{O}}(r)$ of water oxygen with respect to the Fe atom obtained from non-equilibrium simulations $\mathrm{Fe(III)}^{\mathrm{neq}}$ (left panel) and $\mathrm{Fe(II)}_{\mathrm{HS}}^{\mathrm{neq}}$ ($\mathrm{Fe(III)} \rightarrow \mathrm{Fe(II)}_{\mathrm{HS}}$) (middle panel) at different time interval (averaged over 100 trajectories). Comparison of water coordination between three equilibrium state with $\mathrm{Fe(III)}^{\mathrm{neq}}$ at 250 fs (right panel). Black arrows shows the change in water coordination number in the inner shell during the non-equilibrium process. The color codes for the lines are given in the panels.

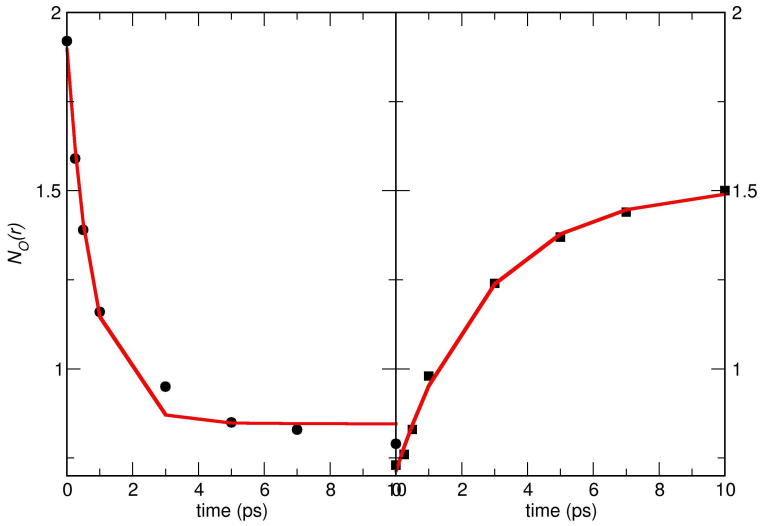

Figure 10: Running coordination number $N_{\mathrm{O}}(r)$ of water oxygen with respect to the Fe atom at 4.75 Å computed at different time intervals during the photo-excitation and fitted to a exponential function: $\mathrm{Fe(III)}^{\mathrm{neq}}$ ($\mathrm{Fe(II)}_{\mathrm{LS}} \rightarrow \mathrm{Fe(III)}$) (left) and $\mathrm{Fe(II)}_{\mathrm{HS}}^{\mathrm{neq}}$ ($\mathrm{Fe(III)} \rightarrow \mathrm{Fe(II)}_{\mathrm{HS}}$) (right). $N_{\mathrm{O}}(r)$ data (black points) and fitted function (solid red curve).

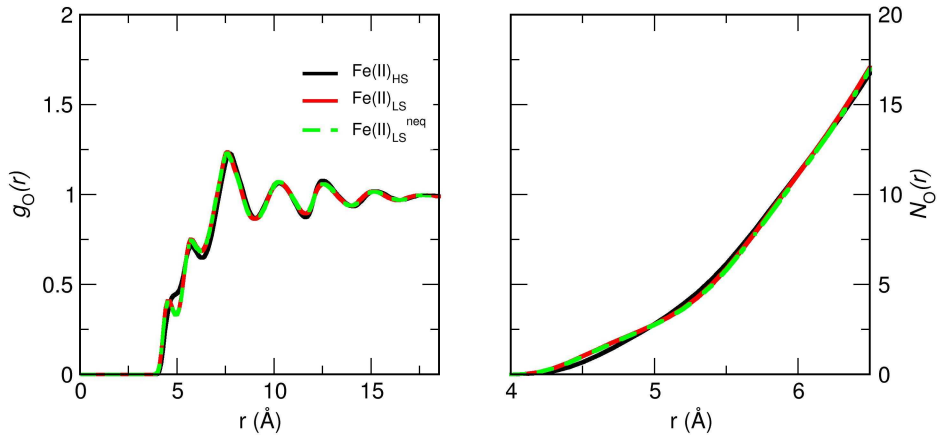

Figure 11: Radial distribution function $g_{\mathrm{O}}(r)$ (left panel) and running coordination number $N_{\mathrm{O}}(r)$ (right panel) of the water oxygen with respect to the metal atom for non-equilibrium $\mathrm{Fe(II)}_{\mathrm{LS}}^{\mathrm{neq}}$ averaged over 25 ps (green dashed line) simulation along with equilibrium $g_{\mathrm{O}}(r)$ and $N_{\mathrm{O}}(r)$ for $\mathrm{Fe(II)}_{\mathrm{LS}}^{\mathrm{eq}}$ (red) and $\mathrm{Fe(III)}_{\mathrm{LS}}^{\mathrm{eq}}$ (black). It is found that full equilibration takes place on the 25 ps time scale.

Residence times: For all three non-equilibrium simulations the water residence time are shorter compared to the corresponding equilibrium simulations. This suggests that during the photo excitation process energy is brought into the system which immediately transfers to the solute and leads the more rapid exchange dynamics of solvent molecules close to the metal center.

3.4 Comparison with Experiment and Previous Simulations

The current simulations provide a framework to discuss several previous investigations of the photocycle in $[\mathrm{Fe(bpy)_3}]$.[1–3,8] Femtosecond time resolved fluorescence spectroscopy showed that starting from the $[\mathrm{Fe(II)_{LS}(bpy)_3}]$ state the system populates the ^{1,3}MLCT (or $[\mathrm{Fe(III)(bpy)_3}]$) excited state with a lifetime of ≤ 200 fs.[1] This lifetime was recently confirmed (150 ± 50 fs) from analysis of femtosecond time resolved X-ray fluorescence spectroscopy.[2] Relaxation via intermediate states, such as a ^{3}T state (with an estimated lifetime of 70 ± 30 fs) leads to the $[\mathrm{Fe(II)_{HS}(bpy)_3}]$ state which has a lifetime of several hundred picoseconds (665 ps).

A combined X-ray emission (XES) and X-ray diffuse (XDS) scattering experiment with a time resolution of 80 ps provided evidence for a change in the solvent density upon excitation of the $[Fe(II)_{LS}(bpy)_3]$ initial state.[3] More recent transient absorption experiments with a time resolution of 50 fs yield relaxation times of 1.1 to 3.4 ps which were associated with vibrational cooling of the metal complex.[48] This compares with time scales of 0.8 and 2.8 ps for the solvent reorganization in the first solvation shell from the present simulations (see Figure 10). Hence, experiments with a time resolution on the multiple 10 ps time scale may be unable to resolve the rapid solvent rearrangement which occurs within picoseconds.

Analysis of the XES and XDS experiments indicated that the density increase occurred on the 100 ps time scale which was linked to ab initio MD simulations run separately for the $[Fe(II)_{LS}(bpy)_3]$ and $[Fe(II)_{HS}(bpy)_3]$ states.[8] These simulations suggested that for the first solvation shell, defined by a radius of 6.3 Å, the water coordination number differs by 2 water molecules, i.e. in the LS and HS state ≈ 17 and ≈ 15 water molecules, respectively, are in the first solvation shell which compares with a conformationally averaged value of 15 and 14 water molecules from the present work. This observation is insofar unexpected as the Fe-N distance increases by 0.2 Å in going from the LS to the HS state and hence *more* space to accommodate water molecules would be available in the HS state. On the other hand it is possible that the charge distribution between $[Fe(II)_{LS}(bpy)_3]$ and $[Fe(II)_{HS}(bpy)_3]$ changes sufficiently to counteract the geometrical changes. Ab initio MD simulations[8] on such systems are very time consuming and therefore in previous work only one trajectory for each state was run for 24 and 4 ps, respectively. Hence, the temporal evolution averaged over a sufficiently large number of snapshots of the system could not be followed.

In the present work the photocycle considered in the fs-TR fluorescence study was followed.[1] Upon excitation to the ^{1,3}MLCT band the degree of solvation decreases on the 250 fs to 500

fs time scale, see Figure 9. As this is a vertical transition with negligible change in the Fe-N geometry (see also Fe-N separations in Tables 2), the origin of the water expulsion is purely electronic, i.e. the charge redistribution drives the process and not the structural change in the $Fe(bpy)_3$ complex. As the system only populates this state for a few hundred fs and decays to $[Fe(II)_{HS}(bpy)_3]$, the change in solvation between the non-equilibrium ^{1,3}MLCT and the equilibrium $[Fe(II)_{HS}(bpy)_3]$ is relevant. As Figure 9 shows, there is negligible difference in the degree of solvation between these two states despite the bond lengthening in $[Fe(II)_{HS}(bpy)_3]$. The number of water molecules expelled from the energized $[Fe(II)_{LS}(bpy)_3]$ state found here is ≈ 1 which differs from the value of 2 which is, however, only based on one quite short QM/MM simulation.[8] It is evident from the present simulations that the degree of solvation decreases on a sub-picosecond time scale and originates from the excitation to the ^{1,3}MLCT band. The experiment reports an estimated increase in the overall solvent density by 0.03 % (no error bar) without accounting for the increased volume and reorientation of the solvent. This was interpreted as a change of 1 to 2 water molecules upon oxidation. The time scale for the solvent exchange is a few picoseconds, which is more rapid than inferred from the experiments but comparable to previous work on CN^- for which the time scale for solvent exchange was also found to be a few picoseconds from both, simulations and NMR experiments.[7,51] Hence it is possible that while the general conclusion of water expulsion upon oxidation can be verified, the time scales found here and in the experiment correspond to different processes. This is confirmed by the observation that the *equilibrium* fluctuations of the solvent shells occur on the few-picosecond time scale. Consequently, electronic excitation will further speed up the solvent dynamics and it is unlikely that the 100 ps time scale found in the experiments directly reflects water exchange dynamics.

In summary, the present simulations suggest that water expulsion occurs between $[Fe(II)_{LS}(bpy)_3]$ and the ^{1,3}MLCT state, is electronically driven, and occurs on a sub-picosecond time scale. Whether or not an intermediate ^{3}T state is included should not affect the present analysis

because the lifetime of this state is very short. The non-equilibrium solvent arrangement of the ^{1,3}MLCT is similar to the [Fe(II)$_{\mathrm{HS}}$(bpy)$_3$] state and hence no further change in the degree of solvation is expected in this transition. It would also be possible to analyze inter- and intramolecular energy flow following electronic excitation as was done previously for the [Ru(bpy)$_3$] complex.[19] Such an analysis was, however, outside the scope of the present work.

4 Conclusions

Atomistic simulations of solvated [Fe(bpy)$_3$] using a validated VALBOND force field provide a detailed picture of the degree of solvation and solvation dynamics involving several spectroscopically characterized states. Upon vertical excitation, which involves significant charge redistribution but only a minimal structural change around the metal center, the degree of solvation decreases. Contrary to that, relaxation from the non-equilibrium excited state to the [Fe(II)$_{\mathrm{HS}}$(bpy)$_3$] state does not change the solvent shell appreciably. Hence, the change in electron distribution governs water expulsion. Relaxation of the non-equilibrium ensemble of the ^{1,3}MLCT state to the equilibrium [Fe(II)$_{\mathrm{HS}}$(bpy)$_3$] state occurs on the picosecond time scale which agrees with recent experiments.[48] The water exchange dynamics in the inner shells close to the metal center take place on the picosecond time scale. Hence, the 100 ps time scale observed experimentally[3] is unlikely to correspond to exchange dynamics of individual water molecules in shells close to the metal center. The use of such force fields allows one to sample the conformational dynamics in a meaningful fashion and to determine averages which can be compared with experimental data and provide atomistic interpretations of the underlying time scales. This is one of the primary advantages of a force field-based approach to characterizing the dynamics of solutes in solution.

5 Acknowledgement

The authors gratefully acknowledge financial support from the Swiss National Science Foundation through the NCCR MUST and grant 200021-117810.

References

(1) Bressler, C.; Milne, C.; Pham, V.-T.; ElNahhas, A.; van der Veen, R. M.; Gawelda, W.; Johnson, S.; Beaud, P.; Grolimund, D.; Kaiser, M. et al. Femtosecond XANES Study of the Light-Induced Spin Crossover Dynamics in an Iron(II) Complex. *Science* **2009**, *323*, 489–492.

(2) Zhang, W.; Alonso-Mori, R.; Bergmann, U.; Bressler, C.; Chollet., M.; Galler, A.; Gawelda, W.; Hadt, R. G.; Hartsock, R. W.; Kroll, T. et al. Tracking Excited-State Charge and Spin Dynamics in Iron Coordination Complexes. *Nature* **2014**, *509*, 345–8.

(3) Haldrup, K.; Vanko, G.; Gawelda, W.; Galler, A.; Doumy, G.; March, A. M.; Kanter, E. P.; Bordage, A.; Dohn, A.; van Driel, T. B. et al. Guest-Host Interactions Investigated by Time-Resolved X-ray Spectroscopies and Scattering at MHz Rates: Solvation Dynamics and Photoinduced Spin Transition in Aqueous [Fe(II)(bipy)$_3$]. *J. Phys. Chem. A* **2012**, *116*, 9878–9887.

(4) Harlang, T. C. B.; Liu, Y.; Gordivska, O.; Fredin, L. A.; Ponseca Jr, C. S.; Huang, P.; Chábera, P.; Kjaer, K. S.; Mateos, H.; Uhlig, J. et al. Iron Sensitizer Converts Light to Electrons with 92% Yield. *Nat. Chem.* **2015**, *7*, 883–889.

(5) Schotte, F.; Lim, M.; Jackson, T. A.; Smirnov, A. V.; Soman, J.; Olson, J. S.; Phillips, G. N., Jr.; Wulff, M.; Anfinrud, P. A. Watching a Protein as it Functions with 150-ps Time-Resolved X-ray Crystallography. *Science* **2003**, *300*, 1944–1947.

(6) Nutt, D.; Meuwly, M. CO Migration in Native and Mutant Myoglobin: Atomistic

Simulations for the Understanding of Protein Function. *Proc. Natl. Acad. Sci.* **2004**, *101*, 5998–6002.

(7) Lee, M. W.; Carr, J. K.; Göllner, M.; Hamm, P.; Meuwly, M. 2D IR Spectra of Cyanide in Water Investigated by Molecular Dynamics Simulations. *J. Chem. Phys.* **2013**, *139*, 054506.

(8) Daku, L. M. L.; Hauser, A. Ab Initio Molecular Dynamics Study of an Aqueous Solution of $[Fe(bpy)_3]Cl_2$ in the Low-Spin and in the High-Spin States. *J. Phys. Chem. Lett.* **2010**, *1*, 1830–1835.

(9) Balzani, V.; Juris, A.; Venturi, M.; Campagna, S.; Serroni, S. Luminescent and Redox-Active Polynuclear Transition Metal Complexes. *Chem. Rev.* **1996**, *96*, 759–833.

(10) Savini, A.; Bellachioma, G.; Ciancaleoni, G.; Zuccaccia, C.; Zuccaccia, D.; Macchioni, A. Iridium(III) Molecular Catalysts for Water Oxidation: the Simpler the Faster. *Chem. Comm.* **2010**, *46*, 9218–9219.

(11) Kalyanasundaram, K.; Gratzel, M. Applications of Functionalized Transition Metal Complexes in Photonic and Optoelectronic Devices. *Coord. Chem. Rev.* **1998**, *177*, 347–414.

(12) Wadman, S. H.; Kroon, J. M.; Bakker, K.; Havenith, R. W. A.; van Klink, G. P. M.; van Koten, G. Cyclometalated Organoruthenium Complexes for Application in Dye-Sensitized Solar Cells. *Organometallics* **2010**, *29*, 1569–1579.

(13) Gaus, M.; Cui, Q.; Elstner, M. Density Functional Tight Binding: Application to Organic and Biological Molecules. *WIREs: Comput Mol Sci* **2014**, *4*, 49–61.

(14) Piquemal, J.-P.; Williams-Hubbard, B.; Fey, N.; Deeth, R. J.; ohad Gresh, N.; Giessner-Prettre, C. Inclusion of the Ligand Field Contribution in a Polarizable Molecular Mechanics: SIBFA-LF. *J. Comp. Chem.* **2003**, *24*, 1963–1970.

(15) Deeth, R. J. General Molecular Mechanics Method for Transition Metal Carboxylates and its Application to t he Multiple Coordination Modes in Mono- and Dinuclear Mn(II) Complexes. *Inorg. Chem.* **2008**, *47*, 6711–6725.

(16) Comba, P.; Hambley, T. W.; Martin, B. *Molecular Modelling of Inorganic Compounds*; VCH, Weinheim, 1995.

(17) Tubert-Brohman, I.; Schmid, M.; Meuwly, M. Molecular Mechanics Force Field for Octahedral Organometallic Compounds with Inclusion of the Trans Influence. *J. Chem. Theo. Comp.* **2009**, *5*, 530–539.

(18) Huang, J.; Häussinger, D.; Gellrich, U.; Seiche, W.; Breit, B.; Meuwly, M. Hydrogen-Bond and Solvent Dynamics in Transition Metal Complexes: A Combined Simulation and NMR-Investigation. *J. Phys. Chem. B* **2012**, *116*, 14406–14415.

(19) Szymczak, J. J.; Hofmann, F. D.; Meuwly, M. Structure and Dynamics of Solvent Shells Around Photoexcited Metal Complexes. *Phys. Chem. Chem. Phys.* **2013**, *15*, 6268–6277.

(20) Brooks, B. R.; Bruccoleri, R. E.; Olafson, B. D.; States, D. J.; Swaminathan, S.; Karplus, M. CHARMM: a Program for Macromolecular Energy, Minimization and Dynamics Calculations. *J. Comp. Chem.* **1983**, *4*, 187–217.

(21) A. D. MacKerell, J.; Bashford, D.; Bellott, M.; R. L. Dunbrack, J.; Evanseck, J. D.; Field, M. J.; Fischer, S.; Gao, J.; Guo, H.; Ha, S. et al. All-Atom Empirical Potential for Molecular Modeling and Dynamics Studies of Proteins. *J. Phys. Chem. B* **1998**, *102*, 3586.

(22) Root, D. M.; Landis, C. R.; Cleveland, T. Valence Bond Concepts Applied to the Molecular Mechanics Description of Molecular Shapes .1. Application to Nonhypervalent Molecules of the p-Block. *J. Am. Chem. Soc.* **1993**, *115*, 4201–4209.

(23) Cleveland, T.; Landis, C. R. Valence Bond Concepts Applied to the Molecular Mechanics Description of Molecular Shapes .2. Applications to Hypervalent Molecules of the p-Block. *J. Am. Chem. Soc.* **1996**, *118*, 6020–6030.

(24) Landis, C. R.; Cleveland, T.; Firman, T. Valence Bond Concepts Applied to the Molecular Mechanics Description of Molecular Shapes. 3. Applications to Transition Metal Alkyls and Hydrides. *J. Am. Chem. Soc.* **1998**, *120*, 2641–2649.

(25) Vanommeslaeghe, K.; Hatcher, E.; Achary, S.; Kundu, S.; Zhong, J.; Shim, E.; Darian, O.; Lopes, P.; Vorobyov, I.; MacKerell Jr, A. D. CHARMM General Force Field: A Force Field for Drug-Like Molecules Compatible with CHARMM All-Atom Additive Biological Force Fields. *J. Comp. Chem.* **2010**, *31*, 671–690.

(26) Reed, A. E.; Weinstock, R. B.; Weinhold, F. Natural Population Analysis. *J. Chem. Phys.* **1985**, *83*, 735–746.

(27) Frisch, M. J.; Trucks, G. W.; Schlegel, H. B.; Scuseria, G. E.; Robb, M. A.; Cheeseman, J. R.; Scalmani, G.; Barone, V.; Mennucci, B.; Petersson, G. A. et al. Gaussian09 Revision D.01. Gaussian Inc. Wallingford CT 2009.

(28) Hehre, W. J.; Ditchfield, R.; Pople, J. A. Self-Consistent Molecular Orbital Methods. XII. Further Extensions of Gaussian-Type Basis Sets for Use in Molecular Orbital Studies of Organic Molecules. *J. Chem. Phys.* **1972**, *56*, 2257–2261.

(29) Becke, A. D. Density-Functional Thermochemistry. III. The Role of Exact Exchange. *J. Chem. Phys.* **1993**, *98*, 5648–5652.

(30) Meuwly, M.; Becker, O. M.; Stote, R.; Karplus, M. NO Rebinding to Myoglobin: A Reactive Molecular Dynamics Study. *Biophys. Chem.* **2002**, *98*, 183–207.

(31) Inskeep, R. G. Infra-red Spectra of Metal Complex Ions Below 600 cm^{-1}: The Spectra

of the Tris Complexes of 1, 10-phenanthroline and 2,2′-bipyridine with the Transition Metals Iron(II) Through zinc(II). *J. Inorg. Nucl. Chem.* **1962**, *24*, 763 – 776.

(32) Gerasimova, T. P.; Katsyuba, S. A. Bipyridine and Phenanthroline IR-Spectral Bands as Indicators of Metal Spin State in Hexacoordinated Complexes of Fe (ii), Ni (ii) and Co (ii). *Dalton Trans.* **2013**, *42*, 1787–1797.

(33) Batten, S. R.; Murray, K. S.; Sinclair, N. J. Tris(2,2′-bipyridyl-*N*,*N*′)iron(II) Diperchlorate. *Acta. Cryst. C* **2000**, *56*, 320.

(34) Figgis, B. N.; Skelton, B. W.; White, A. H. Crystal Structure and E.S.R. of 2,2'-Bipyridylium Tris(2,2'-bipyridyl)iron(III) Tetraperchlorate. *Aust. J. Chem.* **1978**, *31*, 57.

(35) Jorgensen, W. L.; Chandrasekhar, J.; Madura, J. D.; Impey, R. W.; Klein, M. L. Comparison of Simple Potential Functions for Simulating Liquid Water. *J. Chem. Phys.* **1983**, *79*, 926–935.

(36) Ryckaert, J.-P.; Ciccotti, G.; Berendsen, H. J. C. Numerical Integration of the Cartesian Equations of Motion of a System with Constraints: Molecular Dynamics of n-Alkanes. *J. Comp. Phys.* **1977**, *23*, 327–341.

(37) Impey, R. W.; Madden, P. A.; McDonald, I. R. Hydration and Mobility of Ions in Solution. *J. Phys. Chem.* **1983**, *87*, 5071–5083.

(38) Koneshan, S.; Rasaiah, J. C.; Lynden-Bell, R. M.; Lee, S. H. Solvent Structure, Dynamics, and Ion Mobility in Aqueous Solutions at 25 °C. *J. Phys. Chem. B* **1998**, *102*, 4193–4204.

(39) McQuarrie, D. A. *Statistical Mechanics*; Harper's Chemistry Series: New York, 1976.

(40) Allen, M. P.; Tildesley, D. J. *Computer Simulation of Liquids*; Clarendon Press, Oxford, 1987.

(41) Alexander, B. D.; Dines, T. J.; Longhurst, R. W. DFT Calculations of the Structures and Vibrational Spectra of the [Fe(II)(bpy)$_3$] and [Ru(II)(bpy)$_3$] Complexes. *J. Chem. Phys.* **2008**, *352*, 19–27.

(42) Villalba, M. E. C.; Güida, J.; Varetti, E.; Aymonino, P. Infrared Evidence of NO Linkage Photoisomerization in $Na_2[Fe(CN)_5NO].2H_2O$ at Low Temperature: Experimental and Theoretical (DFT) Isotopic Shifts from $^{15}N(O)$, ^{18}O and ^{54}Fe Species. *Spectrochimica Acta Part A: Molecular and Biomolecular Spectroscopy* **2001**, *57*, 367 – 373.

(43) van der Spoel, D.; van Maaren, P. J.; Berendsen, H. J. C. A Systematic Study of Water Models for Molecular Simulation: Derivation of Water Models Optimized for Use with a Reaction Field. *J. Chem. Phys.* **1998**, *108*, 10220–10230.

(44) Ludwig, R. NMR Relaxation Studies in Water-Alcohol Mixtures: the Water-Rich Region.

(45) Moret, M.-E.; Tavernelli, I.; Röthlisberger, U. Combined QM/MM and Classical Molecular Dynamics Study of [Ru(II)(bpy)$_3$] in Water. *J. Phys. Chem. B* **2009**, *113*, 7737–7744.

(46) Park, J.; Lee, T.; Park, J.; Lim, M. Photoexcitation Dynamics of NO-Bound Ferric Myoglobin Investigated by Femtosecond Vibrational Spectroscopy. *J. Phys. Chem. B* **2013**, *117*, 2850–2863.

(47) Elber, R. *Recent Developments in Theoretical Studies of Proteins*; World Scientific: Singapore, New Jersey, London, Hongkong, 1996.

(48) Auböck, G.; Chergui, M. Sub-50-fs Photoinduced Spin Crossover in $[Fe(bpy)3]^{2+}$. *Nat. Chem.* **2015**, *7*, 629–633.

(49) Pham, V.; Penfold, T.; van der Veen, R.; Lima, F.; El Nahhas, A.; Johnson, S.; Beaud, P.; Abela, R.; Bressler, C.; Tavernelli, I. et al. Probing the Transition from

Hydrophilic to Hydrophobic Solvation with Atomic Scale Resolution. *J. Am. Chem. Soc.* **2011**, *133*, 12740–12748.

(50) Bressler, C.; Chergui, M. Molecular Structural Dynamics Probed by Ultrafast X-Ray Absorption Spectroscopy. *Ann. Rev. Phys. Chem.* **2010**, *61*, 263–82.

(51) Lascombe, J.; Perrot, M. Structure and Motion in Water - Analysis of Vibrational and Rotat ional Dynamics of Cyanide Ion in Aqueous-Solution from Infrared and Raman Band Shapes. *Farad. Discuss.* **1978**, *66*, 216–230.

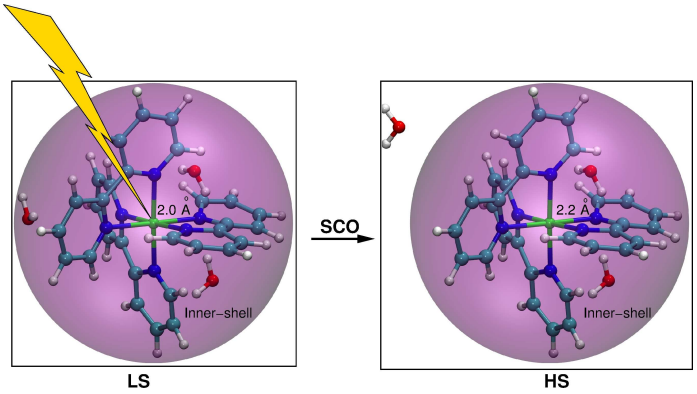

Figure 12: TOC graphics